ADVANCED FUNCTIONAL MATERIALS
www.afm-journal.de
www.MaterialsViews.com

Self-Doped Conjugated Polymeric Nanoassembly by Simplified Process for Optical Cancer Theragnosis

Jeonghun Kim, Eugene Lee, Yoochan Hong, Byeonggwan Kim, Minhee Ku, Dan Heo, Jihye Choi, Jongbeom Na, Jungmok You, Seungjoo Haam, Yong-Min Huh, Jin-Suck Suh, Eunkyoung Kim,* and Jaemoon Yang**

To access smart optical theragnosis for cancer, an easily processable heterocyclic conjugated polymer (poly(sodium3-((3-methyl-3,4-dihydro-2H-thieno[3,4-b][1,4]dioxepin-3-yl)methoxy)propane-1-sulfonate), PPDS) nanoassembly is fabricated by a surfactant-free one-step process, without the laborious ordinary multicoating process. The conjugated nanoassembly, with a self-doped structure, provides strong absorbance in the near-infrared (NIR) range even in a neutral pH medium and exhibits excellent stability (>six months). In addition, the prepared PPDS nanoassembly shows a high photothermal conversion efficiency of 31.4% in organic photothermal nanoparticles. In particular, the PPDS nanoassembly is stably suspended in the biological medium without any additives. Through a simple immobilization with the anti-CD44 antibody, the prepared biomarker-targetable PPDS nanoassembly demonstrates specific targeting toward CD44 (expressed in stem-like cancer cells), allowing NIR absorbance imaging and the efficient targeted photothermal damaging of CD44-expressing cancer cells, from in vitro 3D mammospheres (similar to the practical structure of tumor in the body) to in vivo xenograft mice tumor models (breast cancer and fibrosarcoma). In this study, the most simplified preparation method is for this organic conjugated polymer-based nanoassembly by a molecular approach is reported, and demonstrated as a highly promising optical nanoagent for optical cancer theragnosis.

1. Introduction

In the last decade, photothermal (PT) cancer therapy using near-infrared (NIR) light has been actively investigated with the nanomaterial development of inorganic (e.g., Au,[1–9] Pd,[10,11] $W_{18}O_{49}$,[12] WS_2,[13] CuS,[14] Cu_9S_5,[15] MoS_2,[16] Bi_2Se_3,[17] etc.) and organic (e.g., polyaniline,[18] polypyrrole,[19–22] poly(3,4-ethyl enedioxythiophene):polystyrene sulfonate (PEDOT:PSS),[23,24] carbon materials,[25–28] unit molecules[29,30a]) PT agents. PT therapy method supports the localized ablation of target cancer cells and relative lack of detrimental side effects to the surrounding normal tissues, that are typical for systemic chemotherapy and radiotherapy methods.[7] Therefore, recent studies have been conducted to identify the most suitable PT therapy methods, focusing various aspects including the shape control of PT agents,[9,31] the seeking of new materials,[12–17,23,29,30] the fabrication process,[21,31] the hybridization techniques of enhancing the PT efficiency,[32] and giving magnetic resonance imaging[22] and drug release[24] capabilities.

Among PT agents, organic nanomaterials have received more attentions because the inorganic-based PT agents are nonbiodegradable and generally would remain in the body for long periods of time, causing long-term toxicity.[33] Interestingly, the organic PT agents that have been developed are more economical and better adapted to large-scale production rather than the gold-based nanostructures that

Dr. J. Kim, B. Kim, Dr. J. Choi, J. Na, Prof. S. Haam, Prof. E. Kim
Department of Chemical and Biomolecular Engineering
Yonsei University
Seoul 120-749, Republic of Korea
E-mail: eunkim@yonsei.kr
Dr. J. Kim, B. Kim, J. Na, Prof. E. Kim
Active Polymer Center for Pattern Integration
Yonsei University
Seoul 120-749, Republic of Korea
E. Lee, Dr. Y. Hong, M. Ku, D. Heo, Prof. Y.-M. Huh, Prof. J.-S. Suh
Prof. J. Yang
Department of Radiology, College of Medicine
Yonsei University
Seoul 120-752, Republic of Korea
E-mail: jss@yuhs.ac; 177hum@yuhs.ac
E. Lee, D. Heo, Prof. J.-S. Suh
Nanomedical National Core Research Center
Yonsei University
Seoul 120-752, Republic of Korea
M. Ku, Prof. J.-S. Suh, Prof. J. Yang
Brain Korea 21 Plus Project for Medical Science
College of Medicine, Yonsei University
Seoul 120-752, Republic of Korea
Prof. J. You
Department of Plant and Environmental New Resources
Kyung Hee University
446-701, Republic of Korea
Prof. S. Haam, Prof. Y.-M Huh, Prof. J.-S. Suh, Prof. J. Yang
YUHS-KRIBB Medical Convergence Research Institute
Seoul 120-752, Republic of Korea

DOI: 10.1002/adfm.201500076

have also been tested for PT therapies.[18,34–36] Recently, our report first initiated the use of organic PT nanoagent for the photothermal damage of cancer cells and offered guidance for the utilization of conjugated polymers. This study represented the first fabrication of active and targetable polymeric PT nanoparticles using polyaniline (PAni) as a traditional aromatic conducting polymer.[18] Subsequently, Liu's group reported the polymeric PT ablation with polypyrrole[19–22] and PEDOT:PSS[23,24] nanoparticles as traditional and commercially available conductive polymers.

In spite of recent concentrated developments in PT nanoagent research, a number of unavoidable and uncomfortable difficulties still remain in relation to inorganic and organic PT nanoagents as following: 1) Synthesis: The large-scale synthesis of uniform PT nanoagents is relatively difficult in both inorganic and organic systems. 2) Surfactant treatment: The prepared pristine PT nanoagents need to be coated with the stabilizer (e.g., unit molecules or polymers) to ensure their long-term stability in the medium. 3) Surface functionalization: To give the targeting capability onto cancer, the most PT nanoagents are needed to be functionalized with acidic or basic materials that are able to bind the antibody. 4) PEGylation: Various PEG (polyethylene glycol) derivatives are used to reduce the toxicity and give functionality through wrapping and specific groups, respectively, for almost all PT nanoagents. 5) Multistep processes: The above-mentioned points include multistep works at the experimental preparation stage. 6) Cost: The functionalized specific materials for the stabilization, surface modification, PEGylation, and multistep processes are related with economic considerations.

For the further development of PT nanoagents, thus, the above points should be considered, and the importance of simplifying the systems and finding efficient materials cannot be overemphasized. Till now, although the organic PT nanoagents have already demonstrated some advantages in terms of good stability, relatively low toxicity, and low cost compared to metal-based materials, further efforts are still demanded to develop smart PT nanoagents requiring a simple preparation method, good stability, biocompatibility, targeting capability, and adequate PT properties for efficient cancer therapy.

In order to overcome the critical and remaining problems outlined above, in this study, we here designed and suggest a novel organic optical theragnostic nanoagent using heterocyclic conjugated polymer, PPDS (poly(sodium3-((3-methyl-3,4-dihydro-2H-thieno[3,4-b][1,4]dioxepin-3-yl)methoxy)propane-1-sulfonate)). To evaluate the capability of PPDS as a biomarker-targetable theragnostic probe, colloidal stability and doping state at a physiological condition, as well as biocompatibility and PT efficiency were investigated after the formation of PPDS nanoassembly. On the other hand, breast cancer stem cells (or tumor-initiating cells) characterized by $CD44^+/CD24^-$ surface markers, and retain mammosphere formation and tumorigenic activity have been recently identified in human breast cancer.[37,38] Moreover, these stem-like cancer cells comprised of a heterogeneous cell population are resistant to conventional chemotherapy drugs and radiation.[39] Therefore, research into the application for breast cancers is very important for the clinic. Thus, we conjugated the CD44-specific antibody onto PPDS nanoassembly, setting up these particles to target CD44-expressing cancer cells for NIR imaging and PT ablation. Using a 3D mammosphere in vitro culture system and in vivo tumor xenograft mice model, we observed that these CD44-targetable PPDS nanoassemblies were able to detect and eradicate the tumorigenic CD44-expressing populations in tumor (**Figure 1**).[40,41]

2. Results and Discussion

2.1. Fabrication of PPDS Nanoassembly

To fabricate the organic optical theragnostic nanoagent, PPDS was synthesized through oxidative chemical polymerization. To enhance the hydrophilic properties of poly-ProDOT, a sultone group was introduced to the ProDOT monomers (3-methyl-3,4-dihydro-2*H*-thieno[3,4-b][1,4]dioxepin-3-ol) (Figure 1a and Figure S1, Supporting Information). Subsequently, the modified monomers (ProDOT–sultone) were oxidatively polymerized using excess iron(III) chloride, which produced PPDS in its oxidized state with a molecular weight of 6.5 kDa by matrix assisted laser desorption/ionization time-of-flight mass spectrometry (MALDI-TOF). For the preparation of the dispersed PPDS nanoassembly, the oxidized PPDS was redispersed in phosphate-buffered saline (PBS; pH 7.4) with ultrasonication and the insoluble aggregates were removed by a centrifugation to obtain a clearly dispersed PPDS solution. Finally, self-assembled amphiphilic PPDS nanoassembly in the aqueous phase (pH 7.4) were obtained with a uniform colloidal size of 182.9 ± 9.5 nm, as determined by dynamic light scattering and the morphology investigated by atomic force microscopy (AFM) (Figure 1b). The surface of PPDS nanoassembly was smooth and their size was consistent with the previous results from light scattering. Moreover, the dispersed PPDS nanoassembly could be visualized through dark field microscopy (Figure 1d). This one-step method for the preparation of well-dispersed PT nanoassembly constitutes a greatly simplified approach compared with the previous methods for producing polyaniline,[18] polypyrrole,[19–22] and PEDOT:PSS[23,24] PT nanoparticles, which were formulated through a multicoating process using surfactants. The prepared PPDS nanoassembly was stable and the colloidal stability was maintained for over six months without any severe aggregations (Figure S3a, Supporting Information). The chemical structure of PPDS nanoassembly was confirmed using Fourier-transform infrared (FT-IR) spectroscopy (Figure S2 and Table S1, Supporting Information). The S=O stretching of the sultone and the C=C stretching frequency of the conjugated polymer from PPDS were observed at 1191 and 1537 cm^{-1}, respectively.[42,43] Moreover, due to the outer sultone groups of PPDS nanoassembly (Figure 1e), the zeta-potential was −29.6 ± 7.3 mV and the successful synthesis of redox active PPDS was confirmed with a cyclic voltammogram in an electrochemical study as shown in Figure 1c.

2.2. Physical Characterization of PPDS Nanoassembly

The absorbance spectrum of PPDS nanoassembly appeared to be maximized in the NIR region (Figure S3b, Supporting Information). Generally, the heterocyclic conductive polymers

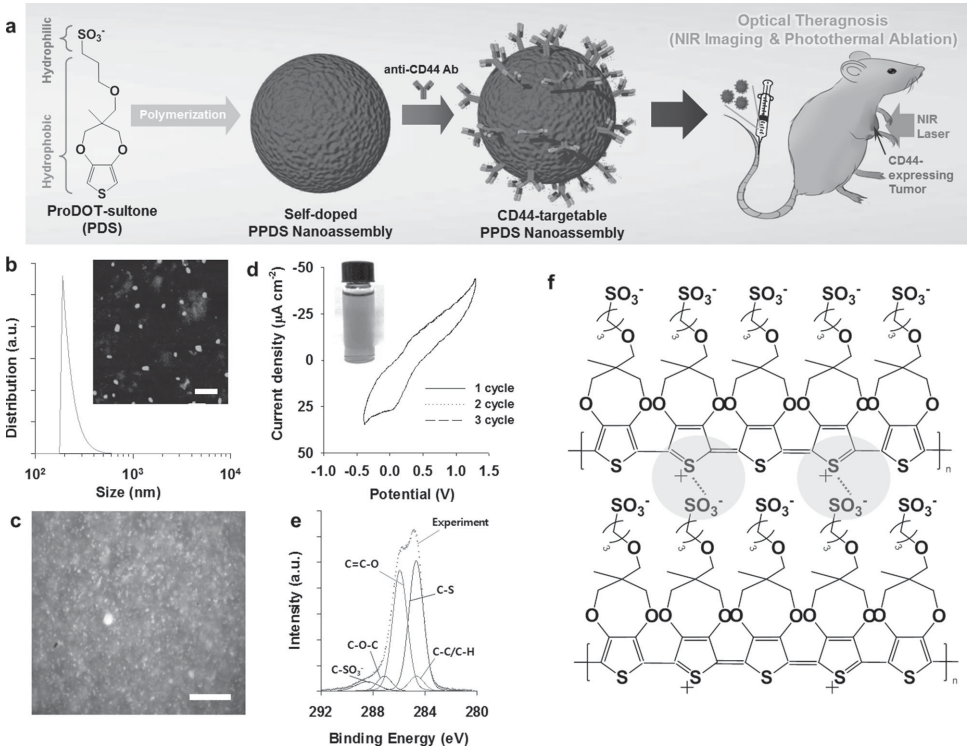

Figure 1. Surfactant-free self-doped PPDS nanoassembly for optical cancer theragnosis. a) Schematic illustration for the fabrication of CD44-targetable PPDS nanoassembly by surfactant-free one-step synthesis and the application to NIR imaging and PT ablation of CD44-expressing cancer cells from xenograft mouse model by the irradiation of NIR laser. b) Size distribution of PPDS nanoassembly by a dynamic laser scattering. Atomic force microscopy image of PPDS nanoassembly is shown in the inset. Scale bar means 500 nm. c) Dark field microscopic image of PPDS nanoassembly. Scale bar means 100 μm. d) Cyclic voltammogram for PPDS nanoassembly on an ITO glass in a H_2O solution containing 0.1 M sodium chloride using a platinum wire at a scan rate of 100 mV s^{-1} (three cycles were tested). A photograph of PPDS nanoassembly dispersed in DW is shown in the inset. e) X-ray photoelectron spectroscopy spectra of C1s for PPDS nanoassembly. Experiment, C—C/C—H, C—S, C═C—O, C—O—C, and C—SO_3^-. f) Molecular structure of self-doped PPDS assembly. Cyanine circles mean self-doping site.

show color through doped and de-doped states which can be controlled through the variation of electrochemical environments.[41,42,44] To observe the pH stability of PPDS nanoassembly, the pH degree of PPDS nanoassembly-dispersed solution was varied and absorbance spectra were obtained as shown in Figure S3b, Supporting Information. Noteworthily, the results showed that the high NIR light absorbance of PPDS (in its oxidized state) was retained at the physiological pH level (pH 7.4) due to the self-doping of PPDS by a strong doping group of $-SO_3^-$ on PPDS itself, which was in contrast with the NIR light absorbance properties of polyaniline (Figure 1f). In accordance with our aim to seek a novel material in this study, we changed the chemical structure of PPDS by introducing of a longer alkyl chain and synthesized ProDOT hexyl sultone (PDHS), as shown in Figure S1, Supporting Information. However, the polymerized PPDHS as a control did not exhibit NIR absorbing peak at pH 7.4, and was precipitated with nonredispersibility due to a conglomerate from the hydrophobic long alkyl chains (Figure S4a, Supporting Information). On the X-ray photoelectron spectroscopy (XPS) spectra and cyclic voltammogram, moreover, the presence and distribution of the sulphur from the sultone group was different in PPDHS, where it showed poor polymerization and nanoparticle formation (Figures S4b and S5, Supporting Information).[45,46] We can conclude therefore that the chemical structure of heterocyclic conductive polymer (PPDS) which can be easily fabricated, simplifying the multistep process for the preparation of optical theragnostic nanoagents. Interestingly, heterocyclic conductive polymer can be chemically modified to achieve the desired functionality, and due to the polaron and bipolaron it exhibits strong and durable NIR absorbance in its oxidized state.[47,48] The chemical structure of PPDS, one of the thiophene derivatives, contains a big and long hydrophobic group of —thiophene–alkyl— and a hydrophilic group of —SO_3. Importantly, due to its amphiphilic properties, we were able to rapidly and easily make water-dispersible PPDS nanoassembly without the help of any surfactants and additives.

The PT characteristics of PPDS nanoassembly as induced by NIR laser (808 nm) illumination were evaluated at various power densities (0.5, 1.0, 2.0, and 5.0 W cm^{-2}). At a power density of 0.5 W cm^{-2}, the PT heating rate of PPDS nanoassembly (4 mg mL^{-1}, 1 mL) was 0.4 °C s^{-1}, it increased linearly with power density (**Figure 2**a). The temperature of PPDS nanoassembly increased up to 52 °C within 2 min at a 5 W cm^{-2} power density (Figure S6, Supporting Information). Moreover, the PT conversion efficiency (η) was calculated using the following equation,[49] and Figure 2b

$$\eta = \frac{hS(T_{max} - T_{surr}) - Q_{dis}}{I\left(1 - 10^{-A_{808}}\right)} \quad (1)$$

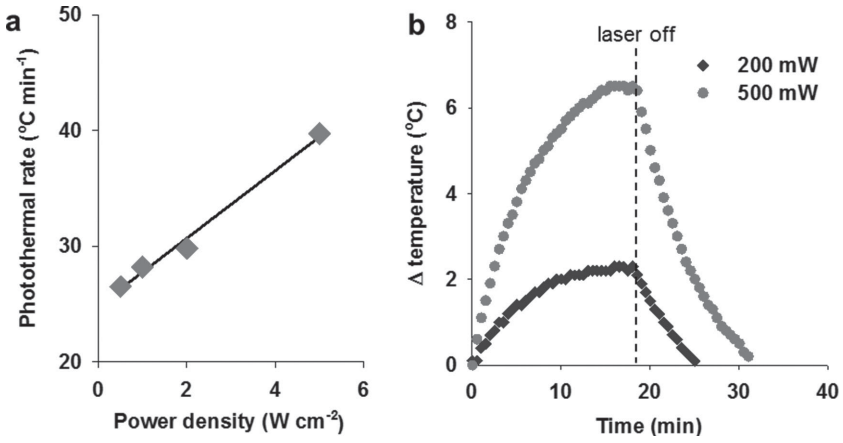

Figure 2. Investigation of PT effect for PPDS nanoassembly. a) PT rates of PPDS nanoassembly at the various power densities of 0.5, 1.0, 2.0, and 5.0 W cm^{-2}. PT rate was calculated from the slope of the temperature increase in the course of 2 min (see Figure S6, Supporting Information). b) Temperature changes (Δ temperature) of PPDS nanoassembly at laser on/off states using different laser power levels for the calculation of the PT efficiency. The power levels of the laser were 200 (circle) and 500 (diamond) mW, respectively. Dotted line means the time of turning-off laser.

where T_{max} and T_{surr} are the equilibrium temperature and ambient temperature of the surroundings, respectively. The h is the heat transfer coefficient and S is the surface area of the sample container. Q_{dis} expresses the heat dissipated from the light absorbed by the quartz sample cell itself, I is the incident laser power, and A_{808} is the absorbance of PPDS nanoassembly at 808 nm. PT conversion efficiency (η) was obtained as 31.4%, which is comparable to other functionalized conjugated polymers and gold nanoparticles (13%–40%).[15,48,50] These results demonstrated that PPDS nanoassemblies were stably suspended in the aqueous phase without a need for additives and possessed the NIR absorbance characteristics required from a PT ablation platform.

2.3. Biocompatibility and PT Ablation Test

In order to evaluate the potential of the nanoassembly for PT anticancer treatment, we assessed the in vitro viability of PPDS nanoassembly for breast cancer cell lines (MDA-MB-231 and MCF7 cells) through a 3-(4,5-dimethylthiazoly-2)-2,5-diphenyltetrazolium bromide (MTT) assay following treatment of PPDS nanoassembly. The treatment of PPDS nanoassembly (up to 20 mg mL^{-1}) for the two cell lines resulted in no cell death or decrease in cellular proliferation (**Figure 3** and Figure S7, Supporting Information). To investigate in vivo biocompatibility, moreover, the immune response after the treatment of PPDS nanoassembly was evaluated through an enzyme-linked immunosorbent assay and the concentration of IL-6 and TNF-α from the sampled whole blood of PPDS-treated mice (n = 3, **Figure 4**). The results demonstrated that CD44-targetable PPDS nanoassembly could be stably applied to in vivo use.

To increase the PT ablation effect, the targeting moiety was then attached to PPDS nanoassembly for specific delivery onto the target cancer cells. Interestingly, the anti-CD44 antibody could be directly conjugated to PPDS nanoassembly through electrostatic physisorption interaction[35] without any of the functionalized surface coating agent. The size of the PPDS nanoassembly after the conjugation of anti-CD44 antibody was slightly increased to 214.6 ± 3.4 nm due to the surface modification and NIR-absorbing property was still maintained as shown in Figure S3c, Supporting Information. Using flow cytometry, we then determined the cell surface expression of CD44 and CD24 on MDA-MB-231 and MCF7 breast cancer cell lines. Cells with a $CD44^+/CD24^-$ expression profile are likely tumor-initiating breast cancer cells, and are therefore a prime target for PT ablation. The majority of MDA-MB-231 cells (96.5%) exhibited the $CD44^+/CD24^-$ expression profile; however, MCF7 cells did not express the $CD44^+/CD24^-$ phenotype (**Figure 5**b). We confirmed the differential expression of CD44 in these two cell lines by treating them with the CD44-targeted PPDS nanoassembly. Through the dark field microscopy, the nanoassembly (viewed as white dots due to light scattering) was seen to associate with MDA-MB-231 cells, but not

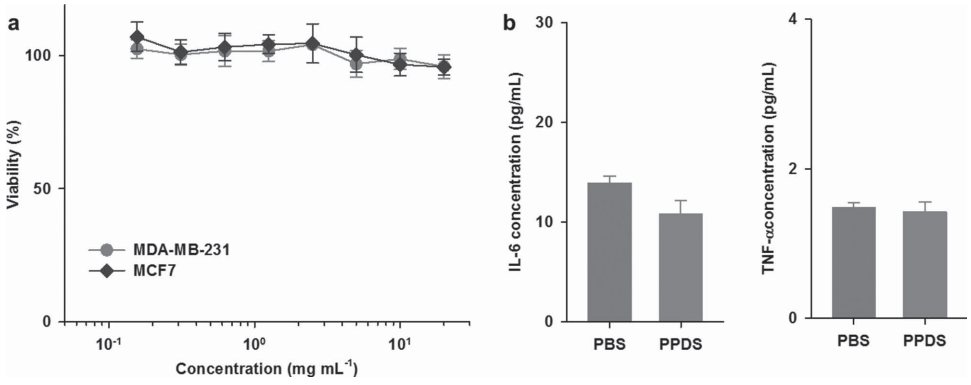

Figure 3. Biocompatibility tests for PPDS nanoassembly. a) Cell viabilities for MDA-MB-231 and MCF7 cells after the treatment of PPDS nanoassembly according to various concentrations. b) In vivo biocompatibility assay graphs IL-6 (left) and TNF-α (right) concentration measured from sampled blood obtained by a control mice (PBS-injection) and PPDS nanoassembly-injected mice, respectively.

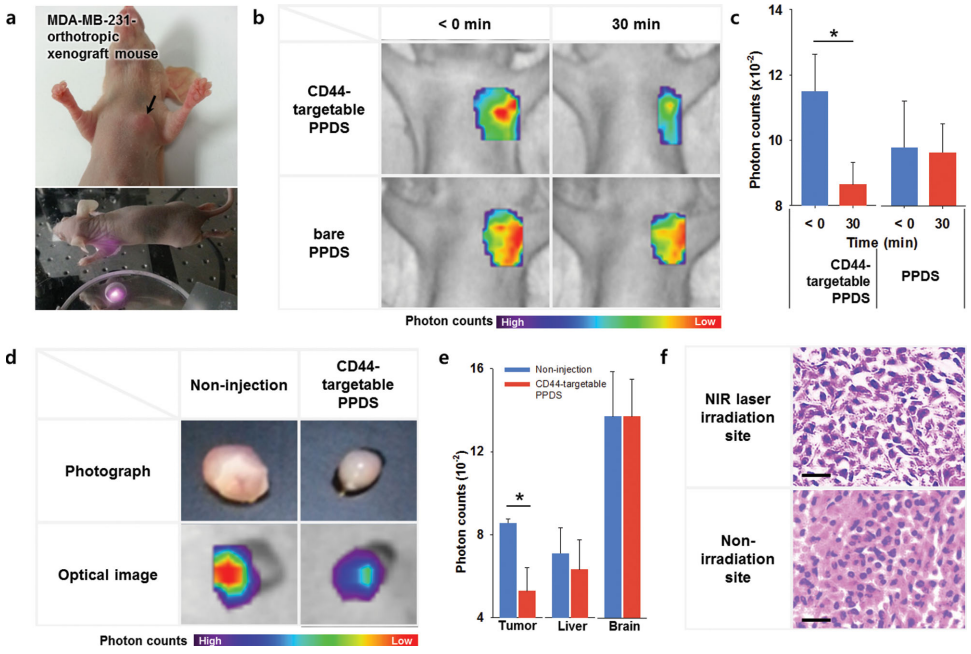

Figure 4. In vivo NIR absorbance imaging and PT effect of CD44-targetable PPDS nanoassembly. a) Photographs of MDA-MB-231 orthotopic xenograft mouse model (upper) and irradiation setting for the PT ablation (lower). b) NIR absorbance images of the tumor-bearing xenograft mice models treated with CD44-targetable PPDS nanoassembly (top images) and bare PPDS nanoassembly (bottom images) for preinjection (<0 min) and postinjection (30 min after the intravenous injection). c) Photon counts graph obtained from b) (*$p < 0.01$). d) Photographs and absorbance images of extracted tumor tissues from tumor-bearing mice model noninjection (left column) and CD44-targetable PPDS nanoassembly treatment (right column). e) Photon counts graphs for extracted tumor, liver, and brain tissues from tumor-bearing mice model noninjection and CD44-targetable PPDS nanoassembly treatment conditions (*$p < 0.01$). f) Hematoxylin and eosin (H&E) staining images for tumor-bearing mice model treated with CD44-targetable PPDS nanoassembly nonirradiation site (upper) and NIR laser (20 W cm^{-2}) irradiation site (lower). Scale bar means 100 μm.

with MCF7 cells by (Figure 5d). Furthermore, the bare PPDS nanoassembly (without anti-CD44 antibody) did not associate with MDA-MB-231 cells (Figure S8, Supporting Information). Thus, CD44-targetable PPDS nanoassembly specifically targeted CD44-expressing cancer cells.

Next, we sought to verify that the CD44-targeted nanoassembly was appropriate for the specific PT ablation of targeted and NIR irradiated cells only. Both MDA-MB-231 and MCF7 cells were treated with CD44-targetable PPDS nanoassembly and specific areas were irradiated with a NIR laser (808 nm). To measure the changes in cell viability, the cells were loaded with calcein-AM and a buffer containing ethidium bromide (EtBr). Live cells retain the calcein dye but exclude EtBr, which causes in bright green fluorescence. By contrast, PT damage prevents calcein dye retention and permeabilizes the cells to EtBr, which results in red fluorescence.[51,52] In Figure 5f, MDA-MB-231 cells irradiated with NIR light (the red dotted line) show red fluorescence as a result of PT damage and cell death. However, the live cells outside the target area are vivid green, indicating that no damage was induced by PPDS nanoassembly in the absence of NIR irradiation. In addition, CD44-deficient MCF7 cells were not damaged by NIR laser exposure because PPDS nanoassemblies were not specifically associated with the cells, demonstrating that NIR laser irradiation alone is not harmful to cells. Thus, CD44-targetable PPDS nanoassembly facilitated the localized PT ablation of CD44$^+$ MDA-MB-231 cells by direct NIR laser irradiation.

2.4. Optical Cancer Theragnosis using Targetable PPDS Nanoassembly

In general, the ability for the formation of 3D mammospheres demonstrates strong self-renewal and tumorigenic potential.[12] Moreover, these 3D structures represent a more realistic in vitro model of tumor architecture. Therefore, we next tested the PT ablation efficacy of PPDS nanoassembly on mammospheres (Figure 5a). Mammospheres of MDA-MB-231 cells presenting acinus-like 3D structures (≈100–150 μm) were grown in a suspension culture (Figure S9a, Supporting Information).[53] CD44 expression of the mammosphere cells was confirmed by immunofluorescence, and CD44$^+$/CD24$^-$ expression profile levels (84.4%) were determined by flow cytometry (Figure S9b,c, Supporting Information). These results were consistent with MDA-MB-231 cells grown in standard adherent conditions. The CD44-targetable PPDS nanoassembly bound to the CD44-expressing mammospheres, as evidenced by the light scattering on the surface of the mammospheres observed through dark field microscopy (Figure 5e).

To test the PT ablation effect of PPDS nanoassembly against the mammospheres, the confluent mammospheres were treated with the CD44-targetable PPDS nanoassembly. When the mammospheres were exposed to weak NIR laser irradiation (8 W cm^{-2}), 50% were killed by the photoinduced heat from PPDS nanoassembly (Figure 5f,g). The live (green fluorescent) cells were only observed at the hemisphere of

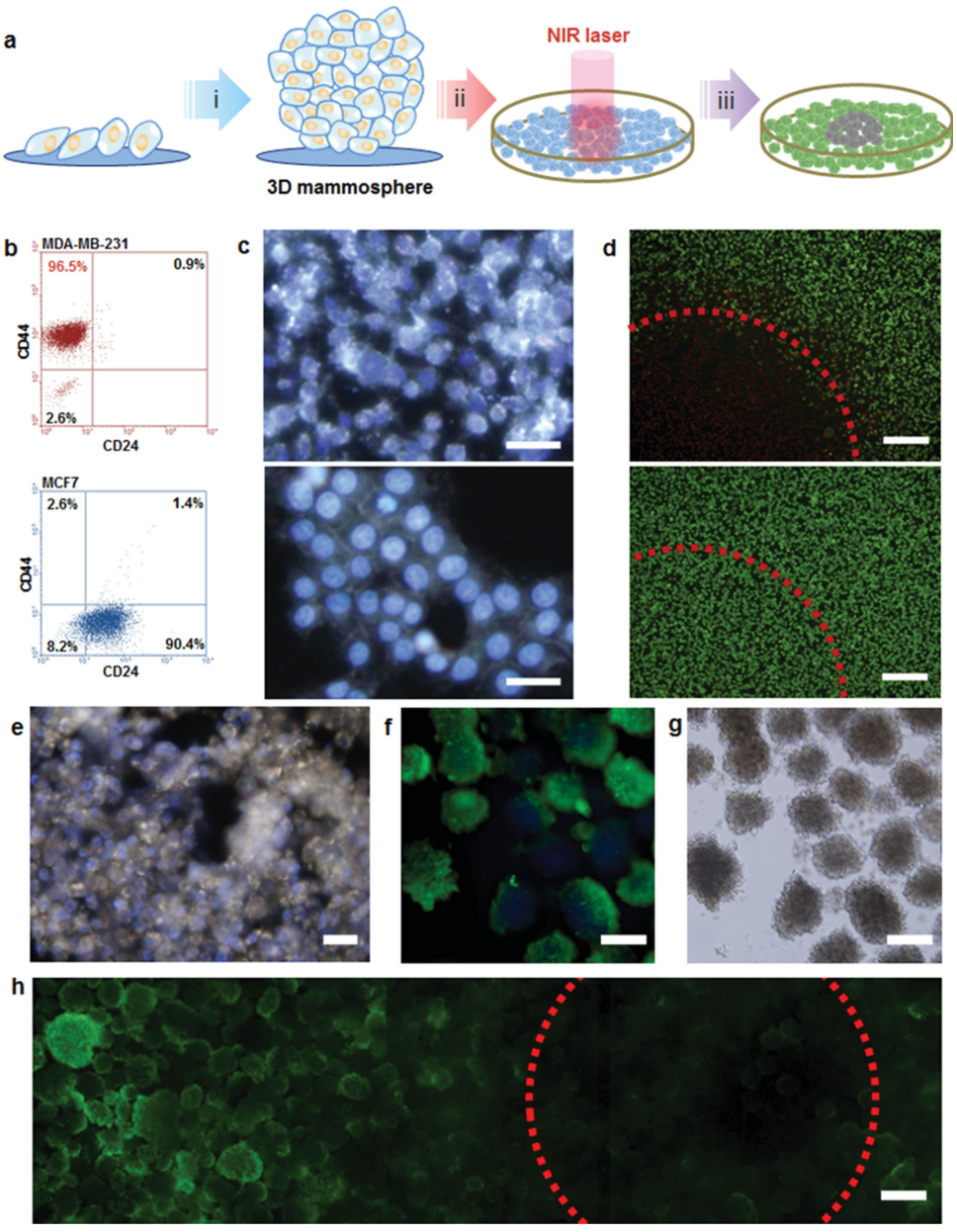

Figure 5. PT ablation of 3D mammospheres by CD44-targetable PPDS nanoassembly. a) Schematic illustration of the PT ablation of breast cancer 3D mammospheres by the combination of CD44-targetable PPDS nanoassembly and NIR laser. i) Cultivation of 3D mammospheres, ii) the treatment of CD44-targetable PPDS nanoassembly and NIR laser irradiation. iii) The confirmation of the PT ablation following cellular staining with calcein-AM and EtBr. The gray-colored area shows the dead 3D mammospheres. b) Flow cytometry analysis of MDA-MB-231 (upper) and MCF7 (lower) cells for CD44 and CD24. c) Dark field microscopic images of MDA-MB-231 (upper) and MCF7 (lower) cells after the treatment of CD44-targetable PPDS assembly. Blue, Hoechst 33342. Scale bar means 20 μm. d) Fluorescence microscopic images of MDA-MB-231 (upper) and MCF7 (lower) cells after treatment with CD44-targeted PPDS assembly and NIR laser (808 nm, 8 W cm^{-2}) irradiation. Red dotted lines indicate the NIR laser irradiated area. Scale bar means 100 μm. e) Dark field microscopic image of MDA-MB-231 mammospheres treated with CD44-targetable PPDS assembly. Blue, Hoechst 33342. Scale bar means 20 μm. f) Fluorescence and g) DIC images for MDA-MB-231 mammospheres treated with CD44-targetable PPDS nanoassembly after NIR laser irradiation (8 W cm^{-2} for 10 min). Scale bar means 100 μm. h) Fluorescence microscopic image for PT ablation potential of CD44-targetable PPDS nanoprobes-treated MDA-MB-231 mammospheres at 20 W cm^{-2} for 10 min. Scale bar = 200 μm.

the mammospheres, and no disruption to the mammosphere morphology was observed through white-light microscopy. By contrast, the irradiation of a stronger NIR light (20 W cm^{-2}) toward the mammospheres treated with CD44-targetable PPDS nanoassembly ablated the mammosphere cells, even in mammospheres larger than 100 μm in diameter (Figure 5h). The unilluminated mammospheres outside the laser target area remained undamaged, as evidenced by calcein fluorescence. Furthermore, the mammospheres that were not treated with CD44-targetable PPDS nanoassembly but were irradiated by the NIR also remained undamaged (Figure S10, Supporting Information). These results demonstrate that CD44-targetable

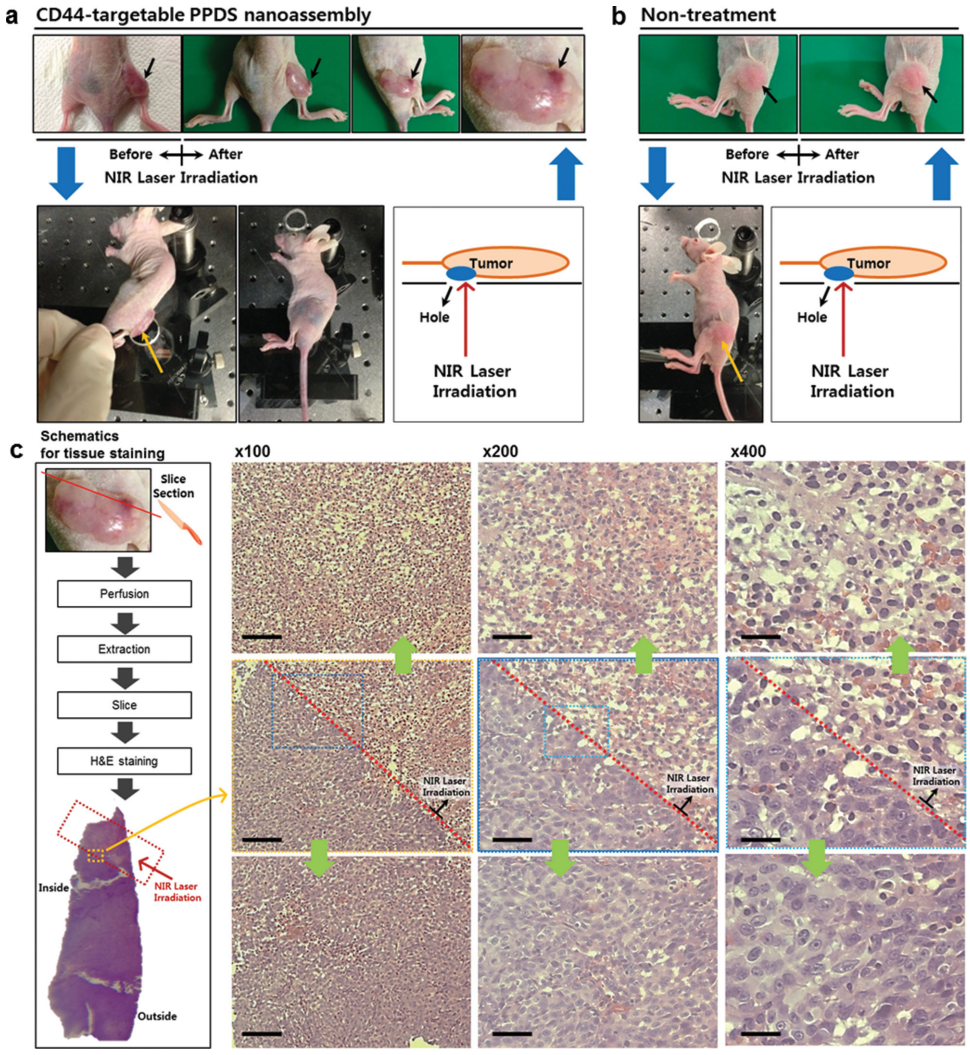

Figure 6. PT damaging of fibrosarcoma xenograft mouse model using CD44-targetable PPDS nanoassembly. PT damaging test for a) CD44-targetable PPDS nanoassembly treatment and b) nontreatment conditions with NIR laser irradiation (2.5 W cm^{-2}, 10 min). c) Schematics for tumor tissue section and H&E staining images of HT1080 tumor-bearing mice model treated with CD44-targetable PPDS nanoassembly after NIR laser irradiation. Upper column: damaged area middle column: boundary area lower column: nondamaged area. Scale bars mean 40 μm.

PPDS nanoassembly can be delivered onto CD44-expressing tumor mammospheres and can facilitate localized cell ablation via directed NIR laser irradiation.

The in vivo targeted delivery and PT ability of the CD44-targetable PPDS nanoassembly was assessed using a tumor-bearing mice model (Figure 4a). 30 min after the injection of the CD44-targetable PPDS nanoassembly into MDA-MB-231 orthotopic xenograft mouse model, NIR absorbance at the breast tumor site was remarkably increased, as shown in Figure 4b–e. However, there was no critical change in the NIR absorbance of the bare PPDS nanoassembly. Moreover, NIR imaging results for the extracted tumor tissue and organs (liver and brain) exhibited tumor-specific delivery of the CD44-targetable PPDS nanoassembly. Therefore, NIR laser light (808 nm, 2.5 W cm^{-2}) was irradiated to the tumor site for 10 min and the PT damage was confirmed on hematoxylin and eosin (H&E) staining microscopic images (Figure 4f). For an extensive confirmation of the targeted delivery and PT effect of the CD44-targetable PPDS nanoassembly, CD44-expressing HT1080 cells (fibrosarcoma) were used to fabricate a xenograft mice model and an in vivo PT ablation study similar to the preceding one. As presented in **Figure 6**, NIR laser on its own could not cause damage at the proximal tumor site (Figure 6b), while the combination of the CD44-targetable PPDS nanoassembly with the NIR laser enabled the ablation of the cancer cells (Figure 6a). In addition, the PT damage of the tumor treated with the CD44-targetable PPDS nanoassembly confirmed on the H&E staining microscopic images (Figure 6c). These results demonstrated that CD44-targetable PPDS nanoassembly could be stably applied to in vivo use as optical theragnostic agents.

3. Conclusion

In summary, we have reported the most simplified and efficient approach for the development of optical theragnostic

nanoassembly based on heterocyclic conductive polymer (PPDS) exhibiting strong and durable NIR absorbance at the physiological pH, and long-term stability from a self-dopable structure. PPDS nanoassembly could be prepared in a well-dispersed solution without any additional surfactants or stabilizers, and presented a comparable PT efficiency of 31.4%. It is noted that PPDS nanoassembly with a sulfonate functional group could target the CD44-expressing cancer cells by direct conjugation of a CD44-specific antibody without surface covering by functionalized materials, and that they specifically adhered to the target cancer cells (both in vitro and in vivo), which enabled the specific PT damaging of the targeted cells. In addition, PPDS nanoassembly showed biocompatibility without the need for complex surface treatments with cell-friendly covering materials, which are unavoidable and necessary processes in all other currently reported studies. The superior PPDS nanoassemblies were applied to the 3D tumor mammospheres and the breast cancer and fibrosarcoma xenograft mice models. PT damaging of the mammospheres indicated that PPDS nanoassembly was effective against CD44-expressing cancer cells, irrespective of the tumor architecture. Moreover, PPDS nanoassembly showed excellent specific targeting of the CD44-expressing cancerous cells, NIR absorbance imaging in vivo, and effective damaging by NIR light irradiation. We can therefore confirm that these novel approaches for simplifying the preparation process of organic optical theragnostic nanoagents through molecular design and structuring offer excellent candidates for the smart optical theragnosis of cancer.

4. Experimental Section

Preparation of CD44-Targetable PPDS Nanoassembly: PPDS was synthesized through oxidative polymerization as shown in Figure S1, Supporting Information, and solid powder was then obtained by filtering and drying. To prepare the water-dispersed PPDS nanoassembly, 100 mg of PPDS powder was first suspended in 20 mL PBS (pH 7.4, 10×10^{-3} M). Following ultrasonication (190 W) for 10 min, the aggregated PPDS clusters were eliminated by centrifugation (3500 rpm for 10 min). The dispersed PPDS nanoassembly was collected and divided with several equivalent volume and some aliquots ($n > 3$) was frozen and dried under a vacuum. The obtained dry PPDS powder was used to quantify the mass concentration of the original PPDS solution. Absorbance of the prepared PPDS nanoassembly was obtained using an absorbance spectrometer (Mecasys UV-2120, Korea). The size and zeta-potential were measured by laser scattering (ELS-Z, Otsuka Electronics, Japan), and the characteristic bands of PPDS nanoassembly were confirmed with Fourier-transform infrared spectroscopy. We utilized the Nanoscope IV controller (Veeco) for AFM imaging of the surface with a tapping model in air at room temperature. A rectangular AFM silicon cantilever (RTESP-Tap300 Metrology Probe, Veeco) was used for tapping-model AFM imagining. Furthermore, an AFM data analysis software was used to obtain a histogram for the grain size of the surface, which was converted from the collected AFM data. For the preparation of the CD44-targetable PPDS nanoassembly, PPDS suspension (4 mg mL^{-1}, 1 mL) was mixed with a 3 µL anti-CD44 antibody solution (Cell Signaling Technology) and incubated at 4 °C for 4 h. The unbound antibodies were eliminated by centrifugation. The final products were resuspended in PBS (1 mL, pH 7.4, 10×10^{-3} M).

Characterization of PT Properties of PPDS Nanoassembly: To investigate the PT potential of PPDS nanoassembly as induced by NIR laser irradiation, 1 mL of a PPDS nanoassembly solution (4 mg mL^{-1}) was prepared. The solution was exposed to a NIR coherent diode laser (808 nm, UM30K, Jenoptik, Germany) for 5 min, and the solution temperature was monitored with a thermocouple (187 true rms multimeters, Fluke, USA). To calculate the PT conversion efficiency, 1 mL of a PPDS nanoassembly solution (1 mg mL^{-1}) was prepared. The solution was exposed to a NIR coherent diode laser for 18 min to be steady-stated, and the temperature of the solution was monitored with a thermocouple.

In Vitro Cell Toxicity of PPDS Nanoassembly: Human breast cancer cell lines MCF-7 and MDA-MB-231 were obtained from the American Tissue Type Culture (ATCC, Rockville, MD, USA). The MCF-7 cells were cultured in a DMEM medium (Gibco, Invitrogen, Grand Island, NY, USA) supplemented with 10% fetal bovine serum (FBS) and 1% antibiotics. MDA-MB-231 cells were cultured in a RPMI 1640 medium (Gibco, Invitrogen) containing 5% FBS and 1% antibiotics. All the cultures were maintained at 37 °C in a 5% CO_2 atmosphere. The cytotoxicity of PPDS was evaluated by a colorimetric assay based on the cellular reduction of MTT (Cell Proliferation Kit I, Roche, Germany) in metabolically active cells. In a typical cell viability experiment, the MCF-7 and MDA-MB-231 cells (10^4 cells per well) were seeded into 96-microwell plates and incubated at 37 °C. After 24 h, the medium was removed, and the cells were incubated with a fresh medium (100 µL) containing various concentrations of PPDS nanoassembly at 37 °C. After the incubation period, the yellow MTT solution was treated, and the formed formazan crystals were solubilized with 10% sodium dodecyl sulfate in 0.01 M HCl. The absorbance of the resulting colored solution was then measured at 575 nm and at 650 nm for reference, using a microplate spectrophotometer (Epoch, BioTek, USA). The cell viability was determined from the intensity ratio of the treated to nontreated control cells and was shown as an average ± standard deviation ($n = 4$). Furthermore, the long-term viability of PPDS nanoassembly was also confirmed using a real-time cell analyzer after 48 h of treatment.

3D Tumor Mammospheres: MDA-MB-231 cells (1×10^6 cells per well) were seeded into ultra-low attachment-coated culture plates (100ϕ, Corning) in a 1:1 DMEM/F12 (Lonza) basal medium freshly supplemented with 5% FBS, 10 ng mL^{-1} epidermal growth factor, 10 µg mL^{-1} insulin, 1 µg mL^{-1} hydrocortisone, and 1% antibiotics (Dontu et al.).[41] The culture medium was changed every two days. The expression of CD44 and CD24 on MDA-MB-231 mammospheres was determined by flow cytometry. Single cells from the mammospheres (1×10^6 cells) were collected, washed three times with a blocking buffer (0.2% FBS and 0.02% sodium azide in PBS, 10×10^{-3} M, and pH 7.4) to prevent nonspecific binding of the antibody, and then incubated with 20 L fluorescein isothiocyanate (FITC)-conjugated rat antimouse CD44 (0.5 µg µL^{-1}) and phycoerythrin (PE)-conjugated rat antimouse CD24 (BD Biosciences) for 30 min at 4 °C. The washed cells were suspended in a 400 µL 4% paraformaldehyde solution and stored at 4 °C prior to the flow cytometry. To determine the affinity of the CD44-targetable PPDS nanoassembly with MDA-MB-231 mammospheres, the cells were seeded at 40 mammospheres per well in a four-well plate and then incubated with CD44-targetable PPDS nanoassembly for 30 min at 4 °C. The treated cells were washed three times with PBS to eliminate the unbound nanoassembly. The cellular binding affinity of the CD44-targetable PPDS nanoassembly against MDA-MB-231 mammospheres was assessed with dark field microscopy after nuclear staining by Hoechst 33342.

In Vitro PT Ablation of Breast Cancer Mammospheres: MDA-MB-231 mammospheres (2×10^2 mammospheres per well) were incubated with a 500 µL CD44-targetable PPDS nanoparticle solution at 4 °C for 30 min in 48-well culture plates. The cells were rinsed with PBS, and a 500 µL phenol red free medium was added to each well. For the laser irradiation experiments, the cells were exposed to a NIR coherent diode laser (808 nm, 8 or 20 W cm^{-2}) for 10 min to induce PT cell damage. The distribution of the live cells was observed with an optical system microscope following cellular staining with calcein-AM and EtBr (1×10^{-6} M) at 37 °C for 30 min.

In Vivo Biocompatibility Tests: The levels of human IL-6 and TNF-α in the blood obtained from mouse models after 24 h from the intravenous

injection of PPDS nanoassembly were determined from triplicate aliquots by an enzyme linked immunoabsorbance assay (ELISA) according to the manufacturer's protocol (Quantikine Immunoassay kit from R&D).

In Vivo NIR-Absorbance Imaging: An orthotopic xenograft mouse model was established with the injection of MDA-MB-231 cells (1×10^7 cells) into the left mammary fat pad of BALB/c nude mice at five weeks of age. To obtain a visual representation of the time-dependent targeting potential, CD44-targetable PPDS or bare PPDS nanoassembly was injected into the tumor-bearing mice ($n = 5$, tumor volume ≈ 500 mm^3) via the tail vein (16 mg mL^{-1}, 50 μL). The delivery of PPDS nanoassembly was imaged by positioning each mouse on an animal plate in the eXplore Optix system (ART Advanced Research Technologies, Montreal). The laser power and count time settings were optimized at 1 μW, and the temporal point spread function (TPSF) integration time was set at 1 s per point. The excitation and emission spots were raster-scanned in 0.5-mm steps over the selected regions of interest to generate emission wavelength scans. A pulsed laser diode (734 nm) was used and the time-dependent absorbance of the CD44-targetable PPDS or bare PPDS nanoassembly was confirmed by measuring the photon counts (i.e., the NIR absorbance intensity). All the experiments were conducted with the approval of the Association for Assessment and Accreditation of Laboratory Animal Care (AAALAC) International.

In Vivo PT Ablation using NIR Laser: The tumor-bearing xenograft mice were anesthetized and CD44-targetable PPDS nanoassembly (16 mg mL^{-1}, 50 μL) were intravenously injected into the tail vein. After 4 h, the tumor site was exposed to a NIR coherent diode laser (8 W cm^{-2}) for 10 min. Subsequently, the mice were sacrificed, and the tumor tissue was excised and fixed using a 4% paraformaldehyde solution. A histological evaluation was conducted using H&E staining. The tissues were embedded in paraffin after being dehydrated with increasing alcohol concentrations and cleared in xylene. Slices (of thickness = 10 μm) were mounted onto glass slides, and for nuclear staining, the slides were placed twice in a container filled with hematoxylin for 10 min. The tissues were rinsed in water for 10 min to remove the hematoxylin, and the cytoplasm was stained with eosin and dehydrated in the same manner as described above. The samples were then rinsed with DI water twice for 5 min. All of the stained tissue sections were analyzed using a virtual microscope (Olympus BX51, Japan) and Olyvia software. For further confirmation of the targeting and PT potential of the CD44-targetable PPDS nanoprobes, CD44-expressing fibrosarcoma HT1080 cells (1×10^6 cells) were used to establish a xenograft mouse model as described above.

Supporting Information

Supporting Information is available from the Wiley Online Library or from the author.

Acknowledgements

J.K. and E.L. contributed equally to this work. This work was supported by a National Research Foundation (NRF) grant funded by the Korean government, Ministry of Education and Science Technology (MEST) (2010-0023202, 2012R1A2A1A01011328), and Ministry of Science, ICT & Future Planning (MSIP) (2007-0056091).

Received: January 7, 2015
Revised: February 3, 2015
Published online: February 26, 2015

[1] L. Dykman, N. Khlebtsov, *Chem. Soc. Rev.* **2012**, *41*, 2256.
[2] Y. Xia, W. Li, C. M. Cobley, J. Chen, X. Xia, Q. Zhang, M. Yang, E. C. Cho, P. K. Brown, *Acc. Chem. Res.* **2011**, *44*, 914.
[3] H. Ke, J. Wang, Z. Dai, Y. Jin, E. Qu, Z. Xing, C. Guo, X. Yue, J. Liu, *Angew. Chem. Int. Ed.* **2011**, *50*, 3017.
[4] H. Liu, T. Liu, X. Wu, L. Li, L. Tan, D. Chen, F. Tang, *Adv. Mater.* **2012**, *24*, 755.
[5] L. Cheng, K. Yang, Y. Li, J. Chen, C. Wang, M. Shao, S.-T. Lee, Z. Liu, *Angew. Chem. Int. Ed.* **2011**, *50*, 7385.
[6] W. Dong, Y. Li, D. Niu, Z. Ma, J. Gu, Y. Chen, W. Zhao, X. Liu, C. Liu, J. Shi, *Adv. Mater.* **2011**, *23*, 5392.
[7] J. Yang, J. Lee, J. Kang, S. J. Oh, H.-J. Ko, J.-H. Son, K. Lee, J.-S. Suh, Y.-M. Huh, S. Haam, *Adv. Mater.* **2009**, *21*, 4339.
[8] J. Lee, J. Yang, H. Ko, S. J. Oh, J. Kang, J.-H. Son, K. Lee, S.-W. Lee, H.-G. Yoon, J.-S. Suh, Y.-M. Huh, S. Haam, *Adv. Funct. Mater.* **2008**, *18*, 258.
[9] E. Kim, J. Yang, J. Choi, J.-S. Suh, Y.-M. Huh, S. Haam, *Nanotechnology* **2009**, *20*, 365602.
[10] X. Huang, S. Tang, X. Mu, Y. Dai, G. Chen, Z. Zhou, F. Ruan, Z. Yang, N. Zheng, *Nat. Nanotechnol.* **2011**, *6*, 28.
[11] X. Huang, S. Tang, J. Yang, Y. Tan, N. Zheng, *J. Am. Chem. Soc.* **2011**, *133*, 15946.
[12] Z. Chen, Q. Wang, H. Wang, L. Zhang, G. Song, L. Song, J. Hu, H. Wang, J. Liu, M. Zhu, D. Zhao, *Adv. Mater.* **2013**, *25*, 2095.
[13] L. Cheng, J. Liu, X. Gu, H. Gong, X. Shi, T. Liu, C. Wang, X. Wang, G. Liu, H. Xing, W. Bu, B. Sun, Z. Liu, *Adv. Mater.* **2014**, *26*, 1886.
[14] Q. Tian, M. Tang, Y. Sun, R. Zou, Z. Chen, M. Zhu, S. Yang, J. Wang, J. Wang, J. Hu, *Adv. Mater.* **2011**, *23*, 3542.
[15] Q. Tian, F. Jiang, R. Zou, Q. Liu, Z. Chen, M. Zhu, S. Yang, J. Wang, J. Wang, J. Hu, *ACS Nano* **2011**, *5*, 9761.
[16] S. S. Chou, B. Kaehr, J. Kim, B. M. Foley, M. De, P. E. Hopkins, J. Huang, C. J. Brinker, V. P. Dravid, *Angew. Chem. Int. Ed.* **2013**, *52*, 4160.
[17] J. Li, F. Jiang, B. Yang, X.-R. Song, Y. Liu, H.-H. Yang, D.-R. Cao, W.-R. Shi, G.-N. Chen, *Sci. Rep.* **2013**, *3*, 1998.
[18] J. Yang, J. Choi, D. Bang, E. Kim, E.-K. Lim, H. Park, J.-S. Suh, K. Lee, K.-H. Yoo, E.-K. Kim, Y.-M. Huh, S. Haam, *Angew. Chem. Int. Ed.* **2011**, *50*, 441.
[19] K. Yang, H. Xu, L. Cheng, C. Sun, J. Wang, Z. Liu, *Adv. Mater.* **2012**, *24*, 5586.
[20] M. Chen, X. Fang, S. Tang, N. Zheng, *Chem. Commun.* **2012**, *48*, 8934.
[21] Z. Zha, X. Yue, Q. Ren, Z. Dai, *Adv. Mater.* **2013**, *25*, 777.
[22] C. Wang, H. Xu, C. Liang, Y. Liu, Z. Li, G. Yang, L. Cheng, Y. Li, Z. Liu, *ACS Nano* **2013**, *7*, 6782.
[23] L. Cheng, K. Yang, Q. Chen, Z. Liu, *ACS Nano* **2012**, *6*, 5605.
[24] H. Gong, L. Cheng, J. Xiang, H. Xu, L. Feng, X. Shi, Z. Liu, *Adv. Funct. Mater.* **2013**, *23*, 6059.
[25] J. T. Robinson, S. M. Tabakman, Y. Liang, H. Wang, H. Sanchez Casalongue, D. Vinh, H. Dai, *J. Am. Chem. Soc.* **2011**, *133*, 6825.
[26] K. Yang, L. Feng, X. Shi, Z. Liu, *Chem. Soc. Rev.* **2013**, *42*, 530.
[27] K. Yang, S. Zhang, G. Zhang, X. Sun, S.-T. Lee, Z. Liu, *Nano Lett.* **2010**, *10*, 3318.
[28] K. Yang, L. Hu, X. Ma, S. Ye, L. Cheng, X. Shi, C. Li, Y. Li, Z. Liu, *Adv. Mater.* **2012**, *24*, 1868.
[29] L. Cheng, W. He, H. Gong, C. Wang, Q. Chen, Z. Cheng, Z. Liu, *Adv. Funct. Mater.* **2013**, *23*, 5893.
[30] a) J. Tian, L. Ding, H.-J. Xu, Z. Shen, H. Ju, L. Jia, L. Bao, J.-S. Yu, *J. Am. Chem. Soc.* **2013**, *135*, 18850; b) Y. Liu, K. Ai, J. Liu, M. Deng, Y. He, L. Lu, *Adv. Mater.* **2013**, *25*, 1353; c) X. Song, Q. Chen, Z. Liu, *Nano Res.* **2014**, DOI 10.1007/s12274–014–0620-y.
[31] Y. Wang, K. C. L. Black, H. Luehmann, W. Li, Y. Zhang, X. Cai, D. Wan, S.-Y. Liu, M. Li, P. Kim, Z.-Y. Li, L. V. Wang, Y. Liu, Y. Xia, *ACS Nano* **2013**, *7*, 2068.
[32] M. Lin, C. Guo, J. Li, D. Zhou, K. Liu, X. Zhang, T. Xu, H. Zhang, L. Wang, B. Yang, *ACS Appl. Mater. Interfaces* **2014**, *6*, 5860.
[33] S. Sharifi, S. Behzadi, S. Laurent, M. L. Forrest, P. Stroeve, M. Mahmoudi, *Chem. Soc. Rev.* **2012**, *41*, 2323.
[34] L. R. Hirsch, R. J. Stafford, J. A. Bankson, S. R. Sershen, B. Rivera, R. E. Price, J. D. Hazle, N. J. Halas, J. L. West, *Proc. Natl. Acad. Sci. USA* **2003**, *100*, 13549.

[35] X. Huang, I. H. El-Sayed, W. Qian, M. A. El-Sayed, *J. Am. Chem. Soc.* **2006**, *128*, 2115.
[36] J. Chen, D. Wang, J. Xi, L. Au, A. Siekkinen, A. Warsen, Z. Y. Li, H. Zhang, Y. Xia, X. Li, *Nano Lett.* **2007**, *7*, 1318.
[37] M. Al-Hajj, M. Wicha, A. Benito-Hernandez, S. Morrison, M. Clarke, *Proc. Natl. Acad. Sci. USA* **2003**, *100*, 3983.
[38] D. Ponti, N. Zaffaroni, C. M. Capelli, G. Daidone, *Eur. J. Cancer* **2006**, *42*, 1219.
[39] L. Lacerda, L. Pusztai, W. A. Woodward, *Drug Resist. Updates* **2010**, *13*, 99.
[40] M. F. Clarke, J. E. Dick, P. B. Dirks, C. J. Eaves, C. H. M. Jamieson, D. L. Jones, J. Visvader, I. L. Weissman, G. M. Wahl, *Cancer Res.* **2006**, *66*, 9339.
[41] G. Dontu, K. Jackson, E. McNicholas, M. Kawamura, W. Abdallah, M. Wicha, *Breast Cancer Res.* **2004**, *6*, R605.
[42] V. Jain, R. Sahoo, S. P. Mishra, J. Sinha, R. Montazami, H. M. Yochum, J. R. Heflin, A. Kumar, *Macromolecules* **2008**, *42*, 135.
[43] J. Kim, J. You, E. Kim, *Macromolecules* **2010**, *43*, 2322.
[44] S. Stafström, J. L. Brédas, A. J. Epstein, H. S. Woo, D. B. Tanner, W. S. Huang, A. G. MacDiarmid, *Phys. Rev. Lett.* **1987**, *59*, 1464.
[45] T. Park, C. Park, B. Kim, H. Shin, E. Kim, *Energy Environ. Sci.* **2013**, *6*, 788.
[46] B. Kim, J. Kim, E. Kim, *Macromolecules* **2011**, *44*, 8791.
[47] P. M. Beaujuge, J. R. Reynolds, *Chem. Rev.* **2010**, *110*, 268.
[48] B. D. Reeves, E. Unur, N. Ananthakrishnan, J. R. Reynolds, *Macromolecules* **2007**, *40*, 5344.
[49] D. K. Roper, W. Ahn, M. Hoepfner, *J. Phys. Chem. C* **2007**, *111*, 3636.
[50] B. Kim, H. Shin, T. Park, H. Lim, E. Kim, *Adv. Mater.* **2013**, *2*, 5483.
[51] S. Fulda, A. M. Gorman, O. Hori, A. Samali, *Int. J. Cell Biol.* **2010**, *2010*, 214074.
[52] M. Boyce, J. Yuan, *Cell Death Differ.* **2006**, *13*, 363.
[53] M. Jo, B. M. Eastman, D. L. Webb, K. Stoletov, R. Klemke, S. L. Gonias, *Cancer Res.* **2010**, *70*, 8948.